A fully reconfigurable series-parallel photovoltaic module for higher energy yields in urban environments

Calcabrini, Andres; Muttillo, Mirco; Weegink, Raoul; Manganiello, Patrizio; Zeman, Miro; Isabella, Olindo

DOI
10.1016/j.renene.2021.07.010

Publication date
2021

Document Version
Final published version

Published in
Renewable Energy

Renewable Energy 179 (2021) 1–11

Contents lists available at ScienceDirect

Renewable Energy

journal homepage: www.elsevier.com/locate/renene

A fully reconfigurable series-parallel photovoltaic module for higher energy yields in urban environments

Andres Calcabrini *, Mirco Muttillo , Raoul Weegink , Patrizio Manganiello , Miro Zeman , Olindo Isabella

Department of Electrical Sustainable Energy, Delft University of Technology, Postbus 5031, 2600 GA, Delft, the Netherlands

ARTICLE INFO

Article history:
Received 23 December 2020
Received in revised form
22 June 2021
Accepted 3 July 2021
Available online 5 July 2021

Keywords:
Reconfigurable PV module
Reconfiguration algorithm
Urban PV
Partial shading
Shading tolerance

ABSTRACT

Photovoltaic modules in the urban environment are very often exposed to uneven illumination conditions. The electrical interconnection between solar cells in a photovoltaic module limits the power that a solar module can generate under partial shading conditions. In this article, we introduce a PV module that is able to dynamically reconfigure the interconnection between its solar cells to minimise conduction and mismatch losses according to the irradiance distribution on its surface. Using an accurate simulation framework, it is determined that a reconfigurable PV module can generate over 12% more energy than a standard PV module with fixed topology and six bypass diodes, and as much energy as a fixed series-parallel module with six parallel strings, but at significantly lower currents. Simulation results are validated experimentally using a photovoltaic module with six reconfigurable blocks of cells controlled by a switching matrix on a high-performance solar flash simulator.

1. Introduction

A large number of photovoltaic (PV) systems in urban environments are often affected by partial shading. Partial shading is usually caused by trees, building structures, soiling and fouling, and it has negative effects on both the electrical performance [1] and the reliability of a PV system [2]. Due to the custom nature of the urban fabric and its random horizons, one module topology with an a-priori determined topology cannot serve all installations. In particular, when a PV system is built with conventional c-Si solar modules, generally made of 60, 72 or 96 solar cells connected in series, a small shadow on the PV module can cause a disproportionate reduction on the electrical output power of the module and the PV system.

Bypass diodes are usually connected in parallel to sub-strings of series-connected cells to prevent hot-spots and reduce power losses when a module is partially shaded [3]. Conventional c-Si modules generally include 3 bypass diodes that become conductive depending on the incident irradiance and the operating point of the PV module. Due to the electrical interconnection between the solar cells and the bypass diodes, most c-Si modules in the market experience a reduction of about 30% in the output power when only 1% of the area of the module is fully shaded [4]. As a consequence, several solutions have been proposed to mitigate the effect of partial shading on a PV system, both at array- and module-level. Main approaches are summarised in Table 1, reporting respective advantages and drawbacks.

One way to improve shade tolerance is to increase the number of bypass diodes in a PV module [5,6]. This approach is relatively simple yet it has some considerable drawbacks: (1) under partial shading the P–V curve can present as many local maxima as bypass diodes in the module, which makes the maximum power point tracking task more complex [7]; and (2) the shade tolerance of modules with many bypass diodes strongly depends on the low forward voltage drop of the bypass diodes. Active bypass elements [8] can be used to reduce voltage and power losses, however, these are still rather expensive [4].

Module level power electronics (MLPE) is a complementary solution that can help in increasing the shade tolerance of PV systems. Micro-inverters [9,10] and power optimisers [11,12] allow to independently perform Maximum Power Point Tracking (MPPT) on each module in the system. Although MLPE devices have some limitations, such as current decoupling [13] in power optimisers and higher system's costs compared to string inverters, these devices improve the system's reliability [14] and significantly increase the electrical yield of partially shaded PV systems [15,16]. Power

* Corresponding author.
E-mail address: a.calcabrini-1@tudelft.nl (A. Calcabrini).

https://doi.org/10.1016/j.renene.2021.07.010

Table 1
Comparison between different approaches for increasing shade tolerance. MLPE stands for module level power electronics.

Approach	Advantages	Disadvantages
MLPE	+ Allows to operate each module at its MPP. + Modular, easily expandable.	- Shading tolerance is limited by module topology. - More expensive than string converters.
Bypass diodes	+ Low cost. + Rather simple to implement. + High performance under uniform illumination.	- Each diode can introduce a different local maximum in the P–V curve. - Limited shade tolerance.
Parallel interconnections	+ High shade tolerance. + Rather simple to implement.	- Low performance under uniform illumination. - Requires power converter with ultra wide input current range.
PV module reconfiguration	+ High shade tolerance. + High performance under uniform illumination.	- Complex implementation. - Requires additional electronics (switching matrix). - Higher cost.

electronics can also be implemented at sub-module level to boost shading tolerance [17,18] at the expense of higher complexity and cost.

A third approach to increase the resilience against shading consists in connecting PV generators in parallel. Some of the most relevant PV array topologies that have been proposed to overcome the poor shading tolerance of series interconnections are total-cross-tied (TCT), series-parallel (SP), bridge-link (BL) and honey-comb (HC) [1,19–23]. Parallel interconnections can also be applied at module-level to improve the shading tolerance of a PV system even further such as in the Tessera module [24] and half-cell PV modules [25].

Whereas under partial shading conditions parallel interconnections help to reduce irradiance mismatch losses, under uniform illumination parallel connected strings may generate high currents which cause high resistive and power conversion losses. In these circumstances, the concept of reconfigurable PV generators allows to adapt the electrical interconnections according to the illumination conditions [26,27]. Reconfigurable PV arrays are usually based on TCT [28–30] and SP [31,32] architectures. Reconfigurable PV generators require a switching matrix that enables the system to alternate between series connections (to minimise resistive and power conversion losses under uniform illumination conditions) and parallel connections (to minimise mismatch losses under partial shading). The switching matrix is controlled by an algorithm that dynamically adapts the system configuration according to the illumination conditions [33].

Reconfiguration is also possible at sub-module level [34]. On the one hand, the design of a reconfigurable PV module involves the development of a reconfiguration matrix and a suitable power converter, naturally this implies higher costs compared to a module with fixed interconnections. On the other hand, a reconfigurable PV module could compensate the higher costs by boosting the energy yield and mitigating the effects of module ageing and degradation, e.g., by disconnecting faulty cells in the module. A simulation study presented in Ref. [35] suggests that reconfigurable modules can deliver 5%–10% more energy than a conventional PV module with 3 bypass diodes considering different degrees of shading and assuming constant power conversion efficiencies. The additional cost of a reconfigurable PV module and its power converter is roughly estimated between €16 and €20 [35]. Considering the current prices of conventional PV modules and module-level power converters, this means that a reconfigurable module could cost around 6%–8% more than a conventional module. However, to make a fair evaluation of the potential of reconfigurable PV modules, the electrical performance should also be compared with shade tolerant fixed module topologies under realistic conditions.

To make a fair evaluation, in this paper we compare modules with the same cell layout but different electrical interconnections. In particular, a highly accurate simulation framework is used to determine the annual DC yield of three PV module topologies: (1) a PV module with 6 bypass diodes, (2) a fixed series-parallel PV module with six strings of cells connected in parallel, and (3) a fully reconfigurable series-parallel PV module with six blocks of series-connected cells. Additionally, a reconfiguration strategy is proposed to dynamically solve the interconnections in the reconfigurable module according to the illumination conditions. Experimental results are presented to support the simulation results.

This article is organised in the following way. In section 2, the design of a fully reconfigurable series-parallel PV module and a reconfiguration algorithm are presented. In section 3, the simulation framework is described and the electrical performance of the different PV module topologies are compared. Finally, in section 4, the simulation results are validated by comparing simulated and measured I–V curves of the reconfigurable PV module in different shading experiments.

2. The series-parallel reconfigurable PV module

The general schematic of the reconfigurable PV topology investigated in this work is presented in Fig. 1. It is considered that one module consists of b blocks of cells, where each block consists of c solar cells connected in series, hence the total number of cells in the module is $b \cdot c$. The switches shown in Fig. 1b constitute a switching matrix that allows to connect the blocks in series and (then) in parallel to obtain different series-parallel module configurations.

A reconfigurable module can adopt a number of different electrical configurations. The configurations of interest (COI) are defined as the subset of all possible electrical configurations which can result in different I–V curves. In a fully reconfigurable series-parallel PV module with b blocks of cells, the number of configurations of interest is given by:

$$COI = \sum_{(s,p)} \frac{b!}{p!\,(s!)^p}, \quad b, s, p \in \mathbb{N} \wedge s \cdot p = b \tag{1}$$

where s represents the number of blocks connected in series forming a string and p represents the number of parallel connected strings. Thus, (s, p) are all possible pairs of natural numbers, whose product equals to the number of blocks b. For example, a reconfigurable module that has 4 blocks has 5 configurations of interest because the pair (s, p) can adopt 3 different values (1,4), (2,2) and (4,1). It is worth to mention that Equation (1) is also valid for fully reconfigurable total-cross-tied topologies [28].

A higher number of blocks allows to build more shade tolerant

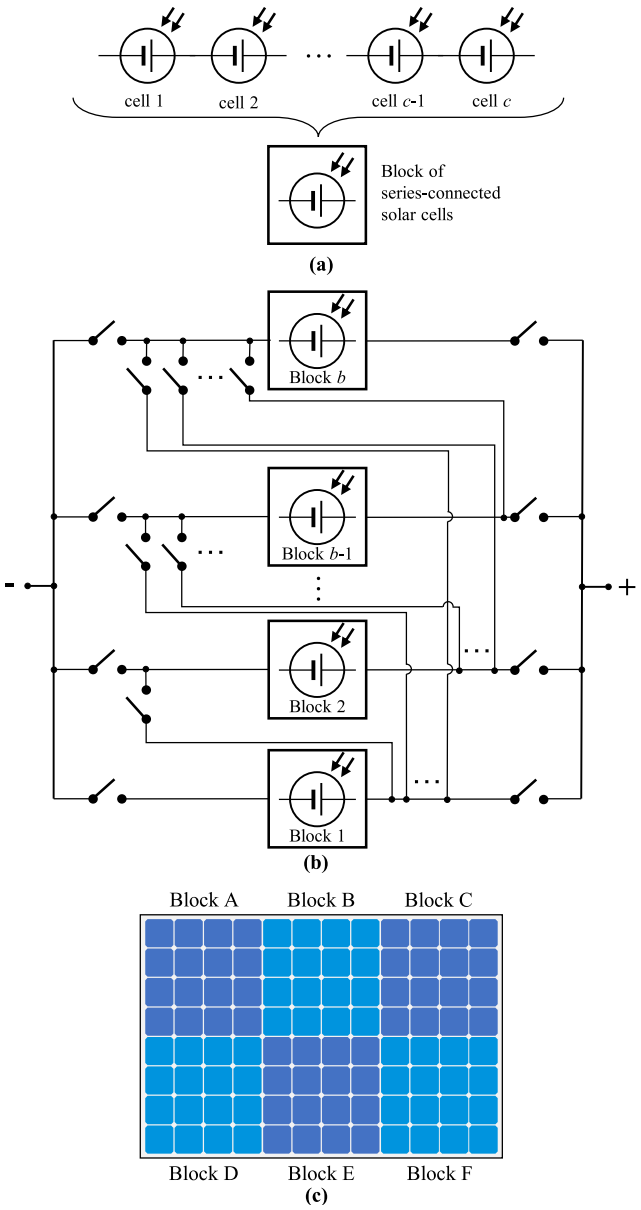

Fig. 1. Reconfigurable series-parallel PV module. (a) One block of c solar cells connected in series. (b) Generic diagram of a fully reconfigurable series-parallel PV modules with b blocks. (c) Layout of the studied reconfigurable module. The module is organised in 6 blocks ($b = 6$), indicated in different shades of blue) of 4 by 4 solar cells connected in series. The positive and negative terminals of each block are connected to the inputs of the switching matrix.

modules [35]. However, it must be noticed that the number of switches required to build a fully reconfigurable series-parallel module increases quadratically with the number of blocks b:

$$\text{switches} = \frac{b\,(b+3)}{2} \tag{2}$$

Equation (2) imposes practical cost and complexity limitations to the design of the switching matrix. Other practical limitations on the design of a reconfigurable PV module to be considered are: (1) the maximum drain-to-source voltage that the switches can tolerate; (2) the maximum allowable continuous drain current of each switch; (3) the maximum number of solar cells per block, that is limited by the reverse characteristics of the solar cells. Aiming to build a reconfigurable PV module prototype with commercially available devices, the proposed module design consists of 96 solar cells, grouped in 6 blocks as shown in Fig. 1c. According to Equation (1), this module can adopt 27 different configurations: (1) one configuration where all blocks are connected in parallel (s1p6); (2) fifteen configurations where three duplets of series-connected blocks are connected in parallel (s2p3); (3) ten configurations where two triplets of series-connected blocks are connected in parallel (s3p2); and (4) one configuration where all the blocks are connected in series (s6p1). All possible configurations are illustrated and enumerated in Fig. B11 in the appendix.

The switching matrix for the proposed module with 6 blocks has 27 switches. In the switching matrix schematic presented in Fig. 1b, all the switches that connect the blocks to the positive and negative terminals can be implemented with a single MOSFET. However, the remaining switches must be bidirectional to avoid shorting blocks of cells through the MOSFET's body diodes.

2.1. The reconfiguration algorithm

Various algorithms have been proposed to control switching matrices [33] in reconfigurable PV modules and arrays. Some algorithms involve periodical I–V curve tracings of each block of cells [36]. Yet in principle, it is possible to control the switching matrix using only current measurements from each block of cells. For most PV modules with c-Si solar cells, the short-circuit current of each block can be considered approximately proportional to the irradiance incident on the least illuminated solar cell in the block. On a second level, temperature and voltage measurements can be used to improve the robustness of the algorithm [37].

In this work, a simple yet effective algorithm is proposed relying only on current measurements. One current sensor is connected in series to each block of cells in Fig. 1a to measure the short-circuit current of each block and estimate the irradiance incident on each block of cells. These current measurements, are dynamically processed by the algorithm that decides which is the optimal module configuration and which switches need to be closed. The algorithm aims to connect blocks of cells with similar irradiances in series and compares the measured short-circuit currents with three predefined threshold constants that are used to determine the optimal module configuration.

The proposed algorithm is depicted in Fig. 2. It begins by measuring the short-circuit current of all six blocks of cells (I_A to I_F). Then, these currents are sorted in descending order and renamed from I_1 to I_6 and six relative differences between the sorted currents are calculated: d_{1-6}, d_{1-3}, d_{4-6}, d_{1-2}, d_{3-4} and d_{5-6}, where:

$$d_{x-y} = \frac{I_x - I_y}{I_x} \tag{3}$$

Next, d_{1-6} is compared to a first threshold value T_1. If the maximum irradiance deviation between all the blocks (d_{1-6}) is lower than T_1, all blocks are connected in series (configuration s6p1). Otherwise, the largest difference between the sorted triplets of currents (d_{1-3} and d_{4-6}) is compared to threshold T_2. If both d_{1-3} and d_{4-6} are smaller than T_2, the best s3p2 configuration is chosen. It is considered that the best s3p2 configuration (among the 10 possible) is determined by the order of the sorted currents. For example, if the order of the sorted currents is $\{I_B, I_C, I_E, I_F, I_A, I_D\}$, then the best s3p2 configuration has one string formed by groups B, C and E connected in parallel to a second string formed by F, A and D. If a solution is not yet found, the algorithm checks if the largest difference between the sorted duplets of currents (d_{1-2}, d_{3-4} and d_{5-6}) is smaller than threshold T_3 and, if so, it chooses the best s2p3 configuration (also determined by the order of the sorted currents).

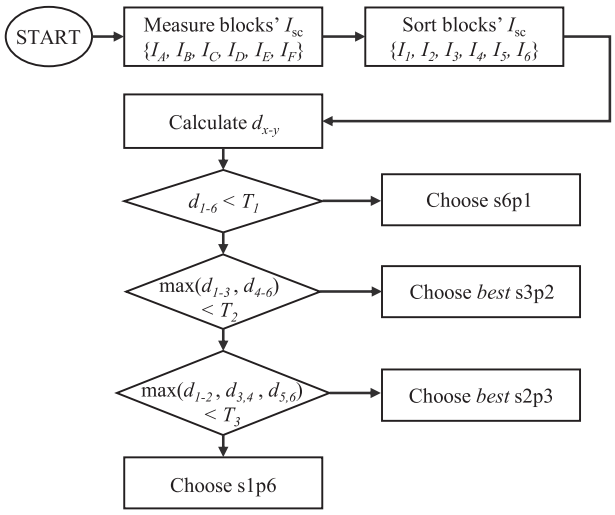

Fig. 2. Block diagram of the proposed reconfiguration algorithm. In every iteration of the algorithm, the currents of the blocks (named from A to F) are sorted in descending order and then renamed from 1 to 6. According to the notation convention, I_1 represents the highest measured current while I_6 represents the lowest measured current.

Finally, if all differences are larger than the established thresholds, configuration s1p6 is chosen and all groups are connected in parallel. In this work, the threshold values are decided based on an optimisation process which considers the electrical characteristics of the solar cells. However, these thresholds can also be adjusted considering the efficiency of the power converter to favour the operation of the reconfigurable PV module in specific voltage and current ranges.

It is worth noting that the proposed algorithm is adaptable to reconfigurable modules with different numbers of blocks. For example, for a module with 8 blocks, 4 sets of configurations would be possible ($1 \times$ s1p8, $105 \times$ s2p4, $35 \times$ s4p2 and $1 \times$ s8p1). In this case, the algorithm would require 3 threshold values and the calculation of 7 relative differences (d_{1-8}, d_{1-4}, d_{4-8}, d_{1-2}, d_{3-4}, d_{5-6} and d_{7-8}).

Since the short-circuit measurements only represent a single point of the I–V curves of each block, even when current measurements are free of noise, the proposed algorithm does not ensure that the best configuration is always the chosen one. It is also evident that the performance of the reconfigurable module depends on the chosen values of the thresholds T_1, T_2 and T_3. With higher threshold values, the algorithm will have a higher tendency to avoid the all-parallel configuration and the reconfigurable module will deliver lower currents. On the other hand, higher threshold values imply a lower shade tolerance. This trade-off brings out the importance of the choice of the threshold values for the algorithm. In practice, there are two additional aspects that should be considered when selecting the threshold values. First, threshold values must be larger than the relative measurement error of the current sensors. Second, in the case of reconfigurable PV modules with bypass diodes, the threshold values should be smaller than the relative difference between the maximum power point current and the short-circuit current of the solar cell to avoid choosing configurations with more than one maximum in the P–V curve.

In the simplest version of the proposed algorithm, the interval between reconfiguration events is fixed and generally ranges between 1 and 5 min. As a result, the variations in the power output of a reconfigurable PV module in timescales shorter than 1 min (e.g. due to rapid changes in irradiance expected during a partially cloudy day) are the same as for conventional PV modules.

Under specific circumstances, the fixed time interval between reconfiguration events could potentially cause hot-spots. For example, if the module is being operated in the all-series configuration (s6p1) and a single cell is totally shaded, the shaded cell could be forced to dissipate a large amount of power until the next reconfiguration event. This problem can be avoided by adding a bypass diode in parallel to each reconfigurable block. Alternatively, the algorithm can be modified to constantly monitor the operating voltage of each block of cells, and generate an interruption if the voltage of one of the blocks suddenly drops. In turn, the interruption would trigger a new reconfiguration event which would find a module configuration where the shaded cell is not reversed biased.

3. Energy yield comparison

3.1. Simulation framework

The additional complexity and cost of a reconfigurable PV module topology compared to fixed module topologies can be justified if the energy yield of the reconfigurable PV module is significantly higher. In this section the potential of a reconfigurable module is assessed by comparing its annual DC yield to that of two fixed module topologies. This comparison is done using a simulation framework which consists of three highly accurate and validated models: (1) an irradiance model to determine the irradiance incident on the solar cells; (2) a thermal model to determine the cells' temperature, and (3) an electrical model to calculate the PV module's I–V curve.

The irradiance on each cell is simulated with Radiance backward ray-tracer [38] considering 2 ambient bounces and using direct normal irradiance (DNI) and diffuse horizontal irradiance (DHI) as inputs for the Perez sky model [39]. For simplicity, it is assumed that all the surfaces surrounding the PV modules are Lambertian reflectors with an average reflectivity of 0.15.

The cell temperature is calculated using the Faiman model [40]. It is considered that the modules are mounted close to the rooftop. The irradiance and wind parameters of Faiman model used in this work ($u_0 = 14.4$ W m^{-2} K^{-1} and $u_1 = 34$ mW m^{-3} s^{-1} K^{-1}) were derived from the empirical coefficients reported in Ref. [41] for close roof mount. For simplicity, Faiman model is decoupled from the electrical model by assuming (only for the thermal calculation) that each cell is operated at its maximum power point (MPP).

The cell temperature and irradiance are combined to calculate the I–V characteristics of a solar cell using the 2-diode electrical equivalent model [42–44]. Both the series (R_s) and parallel (R_p) resistances in the 2-diode model are assumed to be temperature independent, and it is considered that the saturation current of the diodes varies with the cell temperature as described in Ref. [45]. For the simulations, 5-inch solar cells with a maximum power at Standard Test Conditions (STC) of 2.72 W have been considered. The parameters for the 2-diode model given in Table 2, have been fitted using measured I–V curves in dark and at STC of commercially available cells following the approach in Ref. [46]. Finally, the I–V curves of the cells are combined together to calculate the I–V curve of the entire PV module. In this step, the following

Table 2
Solar cell parameters at STC for the double diode model. The parameters are presented in the following order: photogenerated current, ideality factor and saturation current of the first and second diodes, series resistance, shunt resistance and short-circuit current temperature coefficient.

I_{ph0} (A)	n_1 (-)	I_{s1} (pA)	n_2 (-)	I_{s2} (μA)	R_s (mΩ)	R_p (Ω)	$\alpha_{I_{sc}}$ (%/K)
5.67	1	108.9	2	5.645	2.80	20.1	+0.024

electrical losses are included: (1) the equivalent resistance of tabbing wires (2 mΩ) calculated according to Ref. [47]; (2) the resistance of the interconnecting tabs (2 mΩ) calculated considering the length and cross-section of the ribbons [48]; (3) conduction losses in the switches calculated assuming a constant channel resistance (2.1 mΩ) [49]; (4) losses in the bypass diodes calculated considering the diode's I–V characteristics at 25 °C [50]. In practice, bidirectional switches can be implemented with two back-to-back MOSFETs, hence it is considered that the resistance of the bidirectional switches is twice as high as that of the unidirectional switches.

The shading scenario considered in this study is shown in Fig. 3. Results are analysed for the three highlighted module positions in the figure. On each of these positions, the energy yield of the proposed reconfigurable module (6REC) has been simulated and compared against two module topologies with fixed cell interconnections, namely: (1) a module with all 6 blocks connected in series and one bypass diode in parallel to each block (6BPD); and (2) a module with all 6 blocks connected in parallel (6SP). It has been assumed that in all cases modules with ideal local power converters with MPPT capability are used.

3.2. Results

The above-mentioned models were combined to simulate the I–V curves of the different PV modules using 1-min resolution METEONORM climate data [51] for the city of Utrecht, the Netherlands. At this location, during 35% of the daytime (in average), the PV modules only receive diffuse radiation. During these periods of time with no direct light, the reconfigurable PV module is expected to operate mostly in the s6p1 configuration since the irradiance distribution on the PV module surface is rather uniform.

Irradiance simulations results indicate that module positions 1, 2 and 3 in Fig. 3 are exposed to highly uneven[1] illumination during 32%, 14% and 7% of the daytime hours, respectively. Therefore, the DC yield differences between the 6REC and the 6BPD modules are expected to be larger at position 1. At position 3, where the module is barely affected by partial shading, all three module topologies are expected to perform similarly, but REC and 6BPD are expected to generate lower currents than 6SP.

Fig. 4 presents the I–V and P–V curves of the three simulated modules at the most shaded position on the rooftop at different times of the day. In Fig. 4a and b, the reconfigurable module adopts the all-series (27) and all-parallel (1) configurations, respectively. In Fig. 4c, blocks C and F are unshaded, hence the reconfigurable module adopts configuration 4, where these blocks are connected in series (refer to Fig B11).

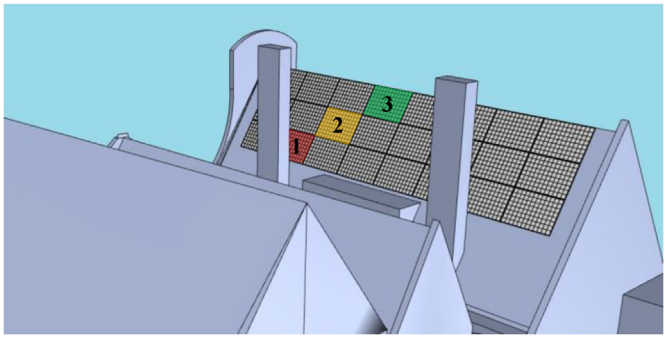

Fig. 3. Simulated PV array. The analysed PV modules are highlighted in different colours. The red module (1) is the most shaded PV module while the green module (3) is the least shaded one.

The DC yield simulation results are summarised in Table 3. The yield of the 6BPD module was calculated assuming two cases: (1) an ideal MPPT algorithm that can always find the absolute MPP (6BPD ideal) and also (2) a more realistic MPPT algorithm that performs an I–V scans every 5 min and might temporarily get stuck at local maxima. The significantly lower performance of the more realistic 6BPD module compared to the ideal case demonstrates the challenge of distinguishing between the true MPP and the local peaks in the P–V curve. In Table 3, the yield of the 6REC module was also calculated assuming two cases: (1) the switching matrix is controlled by an ideal reconfiguration algorithm that always finds the actual best configuration (6REC ideal) and (2) the switching matrix is controlled by the proposed reconfiguration algorithm (6REC algorithm). In both cases, reconfiguration events are triggered every minute.

From the results, it is found that the reconfigurable module (6REC) with the proposed algorithm and the fixed series-parallel module (6SP) perform better than the module with 6 bypass diodes (6BPD) in all the cases. In particular, in the case of the most partially shaded module position, the difference between the 6REC and 6BPD modules is 12.7%. It is worth noticing that, despite the shadows being shorter in summer due to the higher solar elevation, the energy yield difference between the 6SP and the 6BPD modules and between the 6REC and the 6BPD modules become higher in summer months as shown in Fig. 5. Owing to the larger number of clear sky days in summer months than in winter months, PV modules are subject to partial shading for longer periods of time in summer. Similar gains to those given in Table 3 were obtained for simulations performed using METEONORM climate data for Barcelona in the same shading scenario (see Table A5 in appendix). Once again, in Barcelona the shadows cast by the chimneys are even smaller but there are many more clear sky days compared to Utrecht.

In all the cases, the 6SP module achieves a marginally higher yield than the 6REC module despite the expected higher resistive losses at module level. Nevertheless, the 6SP module delivers power at a significantly higher currents than the 6REC module as shown by the histograms in Fig. 6. While the 6SP module can deliver current up to 34 A, the current generated by the 6REC module at the position of the least (Fig. 6a) and most (Fig. 6b) shaded positions almost never exceed 20 A. These observations suggest that a DC-DC converter for the 6REC module has lower input current requirements and can achieve higher conversion efficiencies than a converter for the 6SP module.

As it was mentioned before, the module configuration chosen by the algorithm can sometimes differ from the actual best configuration. Based on the design of the reconfigurable module, the characteristic of the cells in Table 2 and considering the trade-offs discussed in subsection 2.1, a Pareto optimal solution was found with threshold coefficients $T_1 = 3\%$, $T_2 = 5\%$ and $T_3 = 8\%$. Fig. 7 shows the effect of the threshold values on the annual DC yield of the PV module. As expected, lower threshold values favour the all-parallel configuration and imply a higher shading tolerance. With the mentioned threshold values, the match between the algorithm's choice and the actual best configurations varies from 51% at module position 1, to 20% at positions 2, to 13% at position 3. Even so, from the results in Table 3 that correspond to the 6REC modules, it can be concluded that the energy efficiency of the proposed reconfiguration algorithm is over 99.9% for all cases.

[1] In this context, highly uneven illumination means that the irradiance incident on the least illuminated cell in the PV module is at least 50% lower than the irradiance incident on the most illuminated cell.

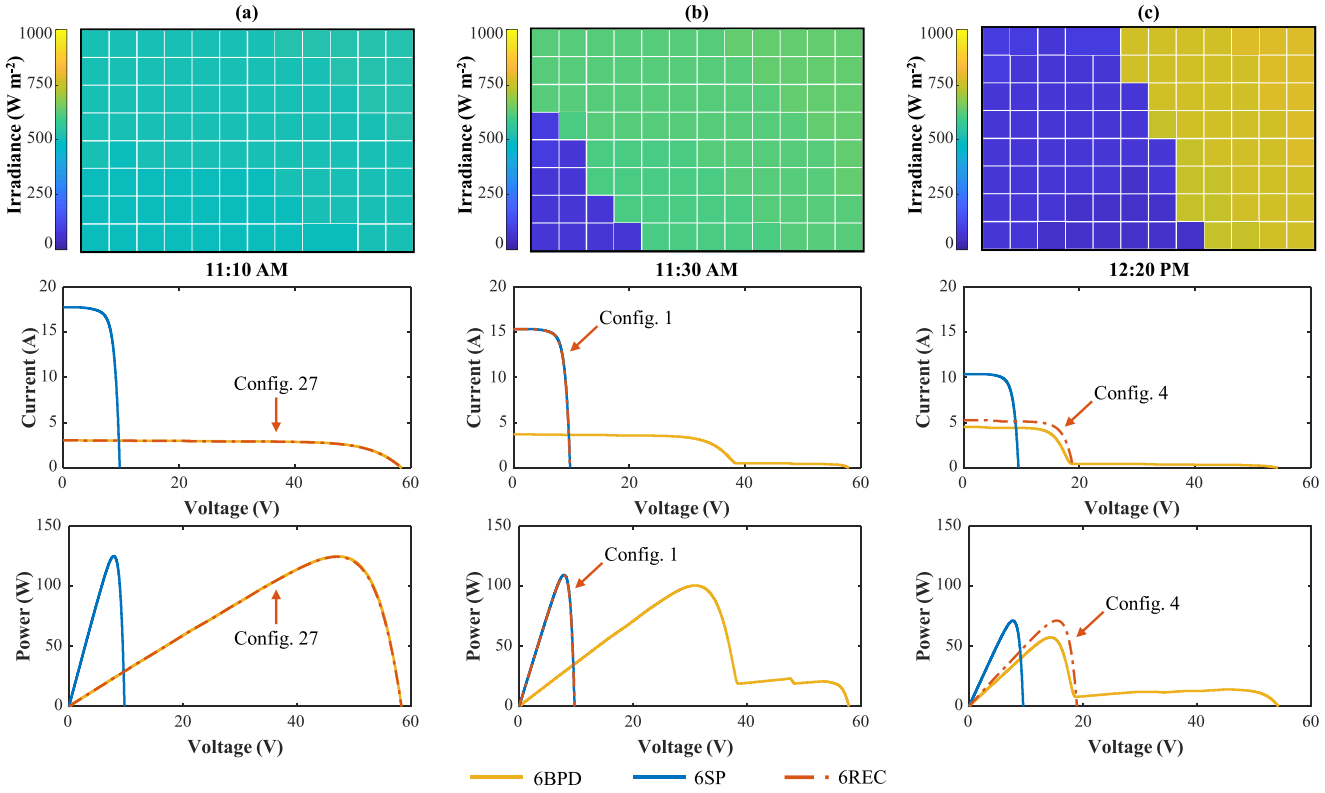

Fig. 4. Simulation results at module position 1 at (a) 11:10 a.m. on the 11th of April, (b) 11:30 a.m. on the 11th of April and (c) 12:20 p.m. on the 11th of April. The configuration chosen by the algorithm at each time is indicated next to the corresponding I–V and P–V curves.

Table 3
Annual specific DC yield comparison of the analysed PV module topologies in different positions on the rooftop shown in Fig. 3 using typical meteorological year data from Utrecht, the Netherlands.

Yield (Wh/Wp)	Position 1	Position 2	Position 3
6BPD ideal	384.80 (ref.)	622.91 (ref.)	776.67 (ref.)
6BPD 5-min scan	364.84 (-5.2%)	615.97 (-1.1%)	773.98 (-0.3%)
6SP	435.06 (+13.1%)	648.24 (+4.1%)	787.32 (+1.4%)
6REC ideal	434.13 (+12.8%)	646.45 (+3.8%)	784.91 (+1.1%)
6REC algorithm	433.74 (+12.7%)	645.97 (+3.7%)	784.68 (+1.0%)

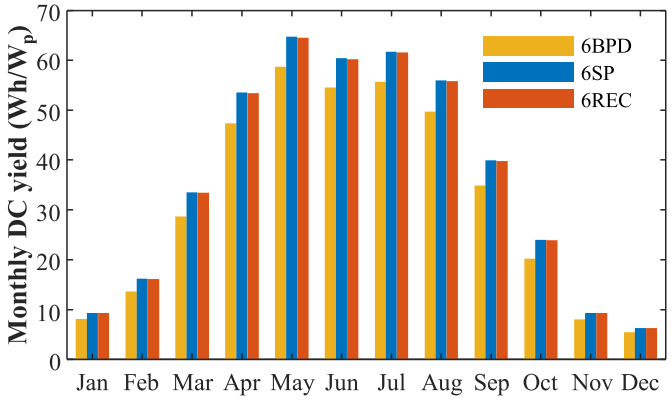

Fig. 5. Monthly yield comparisons of the analysed module topologies in position 1 on the rooftop in Utrecht. It is assumed that the 6BPD module is always operated at the true MPP and that the switching matrix of the 6REC module is controlled by the proposed algorithm.

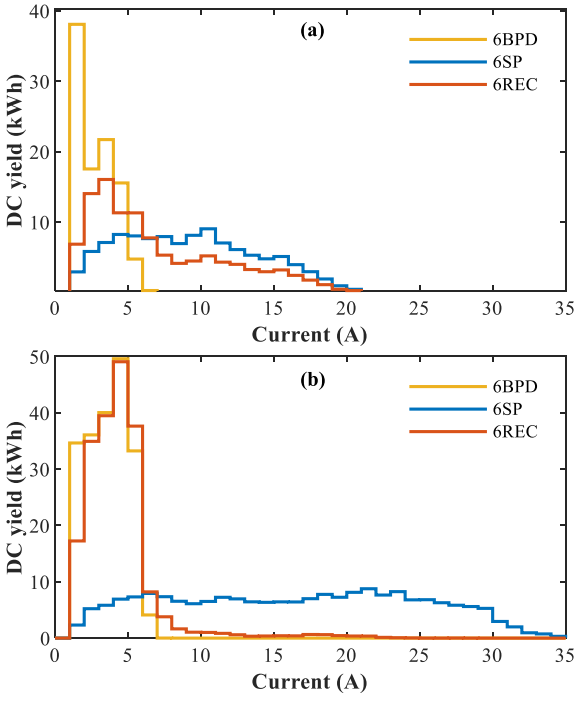

Fig. 6. DC current distribution of the analysed module topologies in Utrecht. (a) Histogram of the DC energy generated by the analysed module topologies as a function of the module's output current for the most shaded position (1) on the rooftop. (b) Histogram of the DC energy generated by the analysed module topologies as a function of the module's output current for the least shaded position (3) on the rooftop. It is assumed that the 6BPD module is always operated at the true MPP and that the switching matrix of the 6REC module is controlled by the proposed algorithm.

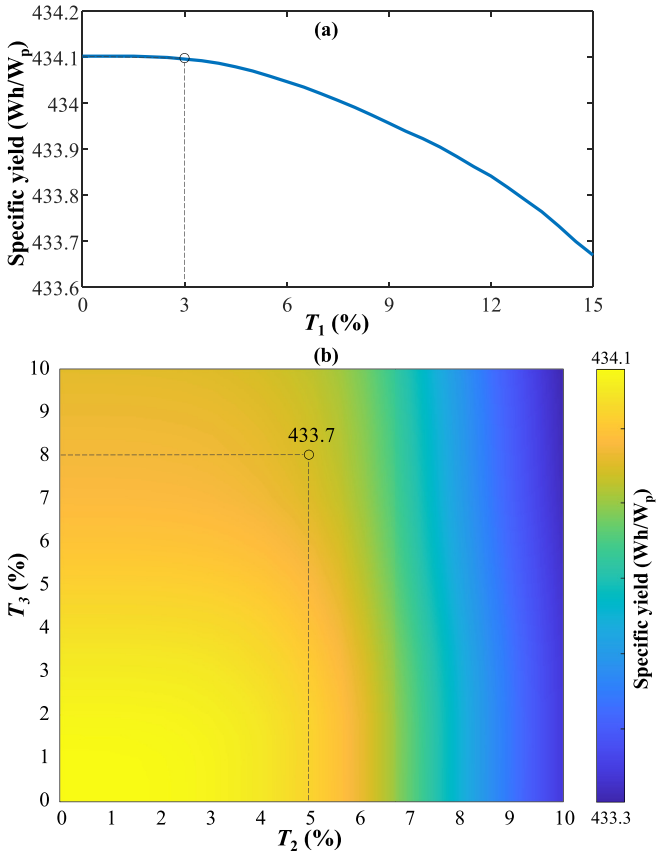

Fig. 7. Annual energy yield of the PV module on rooftop position 1 in Fig. 3 for different threshold values. (a) Effect of T_1 on the annual specific yield considering $T_2 = T_3 = 0\%$. (b) Effect of T_2 and T_3 on the annual specific yield considering $T_1 = 3\%$. The circles indicate the yield obtained with the chosen threshold values.

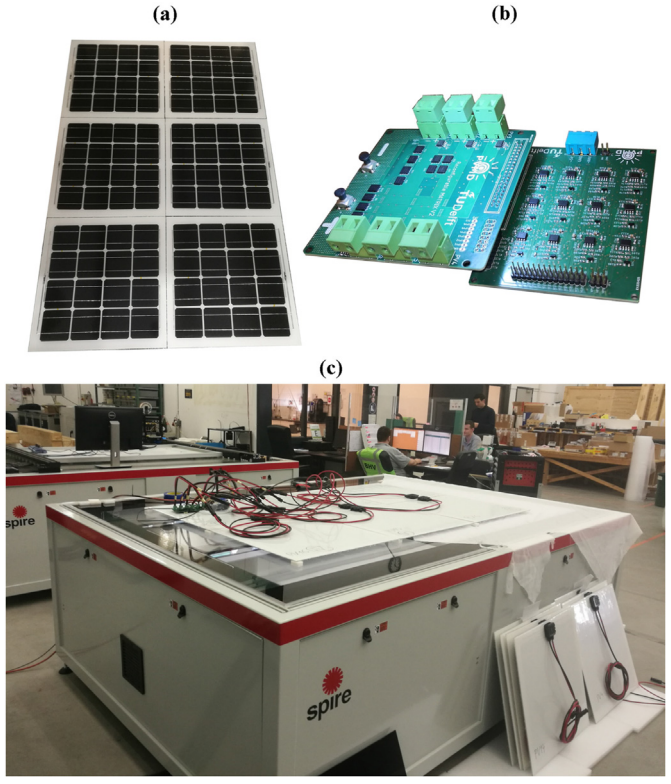

Fig. 8. Experimental setup. (a) Prototype of the reconfigurable module with 6 blocks, each with 16 solar cells (module dimensions are 120 cm by 180 cm). (b) Prototype of the reconfiguration matrix board. (c) Reconfigurable PV module on an EternalSunSpire A + A + A + Xenon Single Long Pulse flash simulator. The image depicts one of the shading experiments.

4. Experimental validation

In order to validate the results presented in this work, a prototype of a reconfigurable module was built and tested on a A + A+A+ flash simulator. The prototype shown in Fig. 8a consists of 6 reconfigurable blocks, each made of 16 series-connected 5-inch mono-crystalline Si solar cells with the parameters listed in Table 2. A reconfiguration board was designed and built (see Fig. 8b) to allow the module to operate in any of its 27 possible configurations. Although the details of the design of the electronic circuit of the switching matrix are out of the scope of this article, it is important to mention that the board includes a microcontroller where the proposed algorithm was programmed and that switches were implemented with the transistors referred in subsection 3.1.

The board and the modules were tested at EternalSunSpire facilities using the A + A+A+ flasher shown in Fig. 8c. From an initial characterisation at STC, it was determined that the 6 reconfigurable blocks of cells have a mismatch lower than 1% in P_{mpp}, I_{sc} and V_{oc}. Later, the blocks were connected to the inputs of the reconfiguration board and the output of the board to the electronic load of the flash tester setup. The I–V curves of the 27 module configurations were measured and simulated for the 3 shading experiments shown in Fig. 9.

During shading experiment A, in Fig. 9a, two blocks of cells were partially shaded with a foil about 30% translucent. It was found that configurations 4, 7 and 14 (refer to Fig. B11) were the best performing. These three configurations are all the s2p3 configurations in which the two shaded blocks are connected in series. Fig. 10 shows the measured and simulated I–V curves of 4 different configurations during experiment A. Results show good agreement between the measured and the simulated maximum power of each configuration. In some of the I–V curves, steps in the I–V curve are visible since bypass diodes were connected in parallel to each block of cells as a protective measure. Nevertheless, it is worth pointing out that reconfigurable modules can be safely operated without any bypass diodes given that the reconfiguration algorithm is robust enough to avoid hot-spots. At the same time, the addition of bypass diodes in these experiments does not affect the maximum power delivered by the optimal configuration (e.g., configuration 4 in Fig. 10). Furthermore, simulations comparing a reconfigurable module with and without bypass diodes revealed a negligible difference in the annual yield (below 0.05%) and that over 99% of the time all bypass diodes are reverse biased at the MPP of the best module configuration.

In experiment B, corner shading was evaluated by covering 3 blocks of cells with a 60% translucent fabric as illustrated in Fig. 9b. In this case, both the measurements and the simulations agree that the best configuration is number 18 (s3p2), where blocks C, E and F are connected in series. In experiment C, blocks D and E were shaded with a foil about 16% translucent and block F was shaded with a foil around 30% translucent. For this shading case, the resulting best configuration is number 17 (s3p2).

Despite the small mismatch between the electrical characteristics of the blocks of cells and other possible sources of error, such as small temperature differences and the non-uniformity of the shading objects, it was determined that the maximum mean absolute error in the simulated maximum power point for all the configurations is 4.0% for shading case A, 2.7% for shading case B

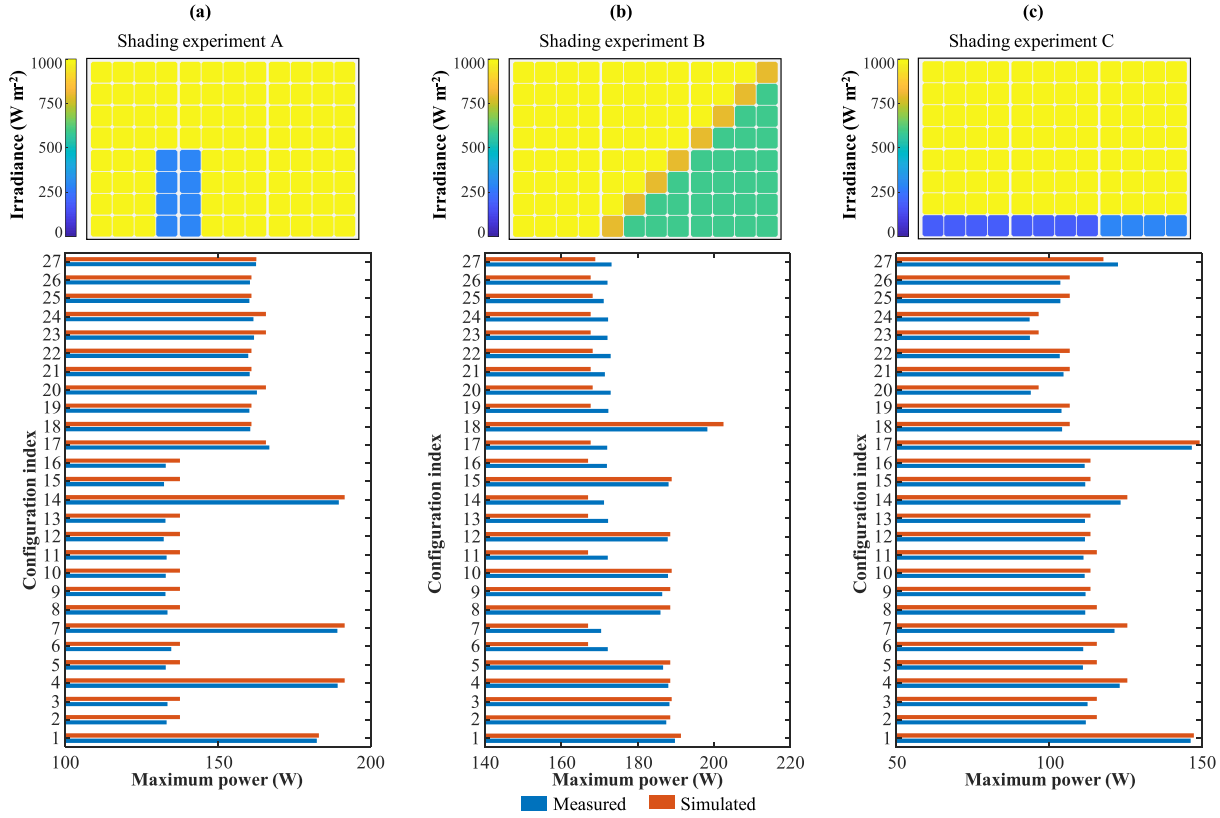

Fig. 9. Measured and simulated maximum power of the reconfigurable PV module. The figure shows the irradiance distribution on the module as well as the simulated and measured maximum power for each of the 27 module configurations for three different shading experiments.

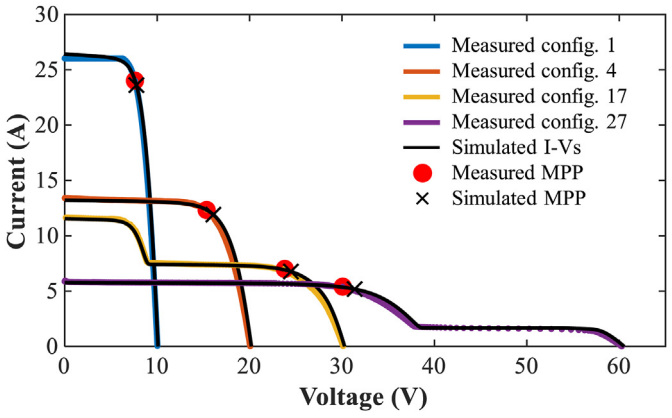

Fig. 10. Measured and simulated I–V curves of configurations 1, 4, 17, and 27 in shading experiment A.

and 4.4% for shading case C. These small errors reflect the high accuracy of the simulation model presented in section 3.1.

The performance of the algorithm was also evaluated for the three shading experiments. Table 4 summarises the measured short-circuit current for blocks A to F, the chosen configuration by algorithm using the measured currents as inputs and the actual best configuration from the power measurements presented in Fig. 9. While in experiment B the algorithm's choice matches the actual best configuration, in experiment A and C the algorithm chooses a sub-optimal configuration. In experiment A, configurations 4 and 14 are equivalent, and therefore the power loss in this case is negligible. On the other hand, in experiment C there is a more relevant discrepancy between the algorithm's choice and the actual best choice. The algorithm chooses configuration 1 (s6p1) instead of the better performing configuration 17 (s3p2). Although the power loss is still low (only 1.3%), configuration 17 delivers lower currents than configuration 1 and it would allow a higher DC-DC conversion efficiency. In experiment C, increasing the value of T_2 would force the algorithm to choose the right configuration, yet it would be possible to find a different shading experiment in which a higher value of T_2 would have the opposite effect. It is therefore concluded that the proposed algorithm cannot avoid this type of situations using only short-circuit current measurement. The use of complementary sensors, such as voltmeters across each block of cells, could help to improve the algorithm's performance. At the same time, voltage measurements could be used to immediately identify when a single block of cells is reversed biased. Thus, the addition of voltage measurements to the reconfiguration algorithm can also ensure the safe operation of a reconfigurable module without any bypass diodes.

Table 4
Algorithm performance for the 3 shading experiments analysed.

	Exp. A	Exp. B	Exp. C
I_A (A)	5.81	5.81	5.79
I_B (A)	5.82	5.82	5.83
I_C (A)	5.79	3.61	5.80
I_D (A)	1.73	5.78	0.97
I_E (A)	1.70	3.58	0.92
I_F (A)	5.73	3.49	1.77
Algorithm's choice	Config. 4	Config. 18	Config. 1
Actual best choice	Config. 14	Config. 18	Config. 17
Relative power loss	−0.1%	0%	−1.3%

It is important to consider that, in practice, the output of the switching matrix is momentarily disconnected from the power converter during each reconfiguration event. This is needed to short-circuit the blocks and measure each of the currents. With the experimental prototype it has been determined that the total time required to measure the short-circuit of each of the 6 blocks and run the algorithm is below 150 ms. Considering a reconfiguration event occurs every minute, the annual loss in the energy yield due to reconfiguration events would be limited to 0.25%. Moreover, simulations suggest that the reconfiguration interval can be increased up to 5 min with a minimal impact on the DC energy yield. In particular, for the 6REC algorithm module in Table 3, the annual yield at position 1 would drop from 433.74 Wh/Wp to 432.89 Wh/Wp if reconfiguration events occurred every 5 min instead of minutely. Under slowly changing shading conditions, it is probably desirable to increase time between reconfiguration events as it could smooth the operation of the power converter with a limited impact on the shading tolerance of the PV module.

As a final note, it must be reminded that in practice there are other sources of partial shading that were not included in the presented simulations, such as soiling, vegetation and bird droppings. Some of these shading sources can have a random effect on the irradiance distribution on the PV module's surface. Random shading can have a disproportionate impact on the output power of modules with fixed interconnections because each block of cell is generally limited by the least illuminated cell. In these cases, the ability of a reconfigurable module to group together blocks of cells that are affected in a similar way would help to reduce the negative effects of random shading.

5. Conclusions

PV systems in the urban environment are frequently partially shaded. Partial shading has a significant impact on the electrical performance of conventional modules, hence shade tolerant PV module topologies are required to increase the yield of urban PV systems. Among the many solutions that have been proposed to increase shading tolerance, reconfigurable PV modules are investigated in this article. In particular, a reconfigurable PV module with 96 solar cells arranged in 6 reconfigurable blocks and its switching matrix have been presented. The proposed module can adopt 27 different series-parallel electrical configurations.

A simulation framework with experimentally validated models has been used to determine the energy yield of the reconfigurable module. Different PV module topologies have been simulated and compared on different positions on the rooftop of a house in Utrecht, the Netherlands. On the one hand, it has been found that when a PV module is 32% of the time shaded, the reconfigurable PV module topology can deliver up to 12.7% more energy than a shade tolerant PV module topology with 6 bypass diodes. Similar results were also obtained for simulations using climate data for Barcelona. On the other hand, a module with 6 strings of cells connected in parallel performs only marginally better than the reconfigurable module in terms of annual DC yield but it delivers much higher electrical currents, which implies a lower DC-DC conversion efficiency. Simulations also allowed to determine that the proposed reconfiguration algorithm based only on short-circuit current measurements can achieve an energy efficiency over 99.9%. Nevertheless, it is recommended to include additional sensors, such as voltage sensors, to increase the robustness and performance of the reconfiguration algorithm.

Finally, a prototype of the proposed PV module and the reconfiguration matrix have been tested using a large area solar flash simulator. The measured electrical performance of all module configurations was evaluated for three shading cases and resulted in an excellent match with the simulation results.

This work paves the way for the realisation of PV-based intelligent energy agents as postulated in our recent work on the arising research field of photovoltatronics [52].

CRediT authorship contribution statement

Andres Calcabrini: Conceptualization, Methodology, Software, Investigation, Writing – original draft, Visualization. **Mirco Muttillo:** Validation, Investigation, Writing – review & editing. **Raoul Weegink:** Software, Validation, Visualization, Writing – review & editing. **Patrizio Manganiello:** Methodology, Supervision, Writing – review & editing. **Miro Zeman:** Supervision, Project administration. **Olindo Isabella:** Conceptualization, Writing – review & editing, Supervision, Project administration.

Declaration of competing interest

The authors declare that they have no known competing financial interests or personal relationships that could have appeared to influence the work reported in this paper.

Acknowledgements

The authors would like to thank EternalSunSpire for allowing the experimental validation of this work at their facilities.

Appendix A. Simulation results in Barcelona

Table A.5
Annual DC yield comparison of the analysed PV module topologies in different positions on the rooftop shown in Fig. 3 using typical meteorological year data from Barcelona, Spain.

Yield (Wh/Wp)	Position 1	Position 2	Position 3
6BPD ideal	611.32 (ref.)	960.18 (ref.)	1216.93 (ref.)
6BPD 5-min scan	592.28 (-3.1%)	950.77 (-1.0%)	1214.56 (-0.2%)
6SP	690.67 (+13.0%)	1003.65 (+4.5%)	1230.73 (+1.1%)
6REC ideal	688.84 (+12.7%)	1000.25 (+4.2%)	1226.18 (+0.8%)
6REC algorithm	688.37 (+12.6%)	999.76 (+4.1%)	1225.89 (+0.7%)

Appendix B Configurations of interest

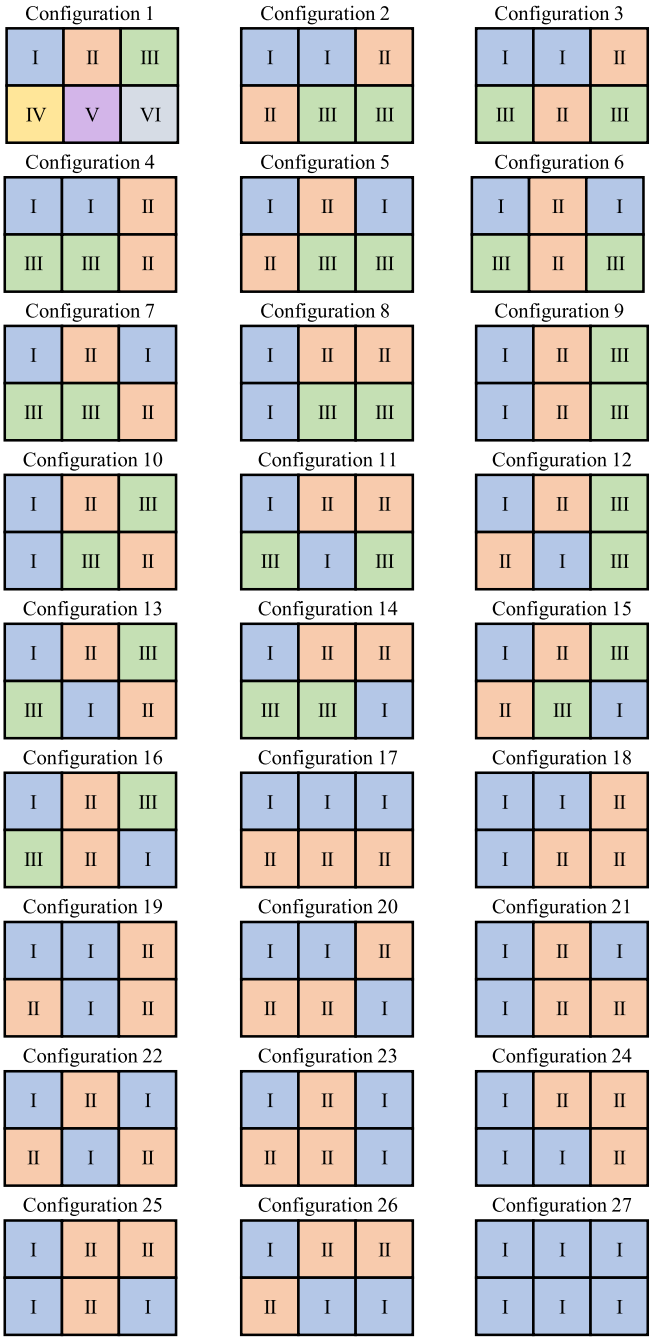

Fig. B.11. Configurations of interest of the proposed PV module with 6 reconfigurable blocks. In each configuration, blocks with the same number (and colour) are connected in series with each other, then the series-connected groups of blocks are connected in parallel. Configuration 1 is also referred to as s1p6 or all-parallel. Configurations 2 to 16 are the 15 possible s2p3 configurations. Configurations 17 to 26 are the 10 possible s3p2 configurations. Configuration 27 is also referred to as s6p1 or all-series.

References

[1] S.R. Pendem, S. Mikkili, Modelling and performance assessment of pv array topologies under partial shading conditions to mitigate the mismatching power losses, Sol. Energy 160 (2018) 303–321.

[2] I. Geisemeyer, F. Fertig, W. Warta, S. Rein, M. Schubert, Prediction of silicon pv module temperature for hot spots and worst case partial shading situations using spatially resolved lock-in thermography, Sol. Energy Mater. Sol. Cell. 120 (2014) 259–269.

[3] W. Herrmann, W. Wiesner, W. Vaassen, Hot spot investigations on pv modules-new concepts for a test standard and consequences for module design with respect to bypass diodes, in: Conference Record of the Twenty Sixth IEEE Photovoltaic Specialists Conference-1997, IEEE, 1997, pp. 1129–1132.

[4] B.B. Pannebakker, A.C. de Waal, W.G. van Sark, Photovoltaics in the shade: one bypass diode per solar cell revisited, Prog. Photovoltaics Res. Appl. 25 (10) (2017) 836–849.

[5] E.S. Hasyim, S. Wenham, M. Green, Shadow tolerance of modules incorporating integral bypass diode solar cells, Sol. Cell. 19 (2) (1986) 109–122.

[6] H. Hanifi, M. Pander, B. Jaeckel, J. Schneider, A. Bakhtiari, W. Maier, A novel electrical approach to protect pv modules under various partial shading situations, Sol. Energy 193 (2019) 814–819.

[7] H. Patel, V. Agarwal, Maximum power point tracking scheme for pv systems operating under partially shaded conditions, IEEE Trans. Ind. Electron. 55 (4) (2008) 1689–1698.

[8] P. Bauwens, J. Doutreloigne, Reducing partial shading power loss with an integrated smart bypass, Sol. Energy 103 (2014) 134–142.

[9] H.A. Sher, K.E. Addoweesh, Micro-inverters—promising solutions in solar photovoltaics, Energy for Sustainable Development 16 (4) (2012) 389–400.

[10] R. Hasan, S. Mekhilef, M. Seyedmahmoudian, B. Horan, Grid-connected isolated pv microinverters: a review, Renew. Sustain. Energy Rev. 67 (2017) 1065–1080.

[11] S.M. MacAlpine, R.W. Erickson, M.J. Brandemuehl, Characterization of power optimizer potential to increase energy capture in photovoltaic systems operating under nonuniform conditions, IEEE Trans. Power Electron. 28 (6) (2012) 2936–2945.

[12] M.Z. Ramli, Z. Salam, Performance evaluation of dc power optimizer (dcpo) for photovoltaic (pv) system during partial shading, Renew. Energy 139 (2019) 1336–1354.

[13] R. Orduz, J. Solórzano, M.Á. Egido, E. Román, Analytical study and evaluation results of power optimizers for distributed power conditioning in photovoltaic arrays, Prog. Photovoltaics Res. Appl. 21 (3) (2013) 359–373.

[14] C. Olalla, D. Maksimovic, C. Deline, L. Martinez-Salamero, Impact of distributed power electronics on the lifetime and reliability of pv systems, Prog. Photovoltaics Res. Appl. 25 (10) (2017) 821–835.

[15] C. Deline, B. Marion, J. Granata, S. Gonzalez, Performance and Economic Analysis of Distributed Power Electronics in Photovoltaic Systems, Tech. Rep. NREL/TP-5200-50003, National Renewable Energy Lab.(NREL), Golden, CO (United States), 2011.

[16] K. Sinapis, C. Tzikas, G. Litjens, M. Van den Donker, W. Folkerts, W. Van Sark, A. Smets, A comprehensive study on partial shading response of c-si modules and yield modeling of string inverter and module level power electronics, Sol. Energy 135 (2016) 731–741.

[17] P. Mazumdar, P.N. Enjeti, R.S. Balog, Smart pv modules - design considerations, in: 2012 IEEE International Conference on Power Electronics, Drives and Energy Systems (PEDES), IEEE, 2012, pp. 1–6.

[18] Q. Gao, Y. Zhang, Y. Yu, Z. Liu, A direct current-voltage measurement method for smart photovoltaic modules with submodule level power optimizers, Sol. Energy 167 (2018) 52–60.

[19] A. Bidram, A. Davoudi, R.S. Balog, Control and circuit techniques to mitigate partial shading effects in photovoltaic arrays, IEEE.J.Photovoltaics 2 (4) (2012) 532–546.

[20] B.I. Rani, G.S. Ilango, C. Nagamani, Enhanced power generation from pv array under partial shading conditions by shade dispersion using su do ku configuration, IEEE Transactions on sustainable energy 4 (3) (2013) 594–601.

[21] F. Belhachat, C. Larbes, Modeling, analysis and comparison of solar photovoltaic array configurations under partial shading conditions, Sol. Energy 120 (2015) 399–418.

[22] N. Mishra, A.S. Yadav, R. Pachauri, Y.K. Chauhan, V.K. Yadav, Performance enhancement of pv system using proposed array topologies under various shadow patterns, Sol. Energy 157 (2017) 641–656.

[23] O. Bingöl, B. Özkaya, Analysis and comparison of different pv array configurations under partial shading conditions, Sol. Energy 160 (2018) 336–343.

[24] A.J. Carr, K. de Groot, M.J. Jansen, E. Bende, J. van Roosmalen, L. Okel, W. Eerenstein, R. Jonkman, R. van der Sanden, J. Bakker, et al., Tessera: scalable, shade robust module, in: 2015 IEEE 42nd Photovoltaic Specialist Conference (PVSC), IEEE, 2015, pp. 1–5, https://doi.org/10.1109/PVSC.2015.7356286.

[25] H. Hanifi, J. Schneider, J. Bagdahn, Reduced shading effect on half-cell modules–measurement and simulation, in: 31th European Photovoltaic Solar Energy Conference and Exhibition, Hamburg, 2015, pp. 2529–2533, https://doi.org/10.4229/EUPVSEC20152015-5CV.2.25.

[26] R.A. Sherif, K.S. Boutros, Solar Module Array with Reconfigurable Tile, uS Patent 6,350,944, Feb. 26 2002.

[27] C. Chang, Solar Cell Array Having Lattice or Matrix Structure and Method of Arranging Solar Cells and Panels, uS Patent 6,635,817, Oct. 21 2003.

[28] G. Velasco-Quesada, F. Guinjoan-Gispert, R. Piqué-López, M. Román-Lumbreras, A. Conesa-Roca, Electrical pv array reconfiguration strategy for energy extraction improvement in grid-connected pv systems, IEEE Trans. Ind. Electron. 56 (11) (2009) 4319–4331.

[29] S. Vemuru, P. Singh, M. Niamat, Analysis of photovoltaic array with reconfigurable modules under partial shading, in: 2012 38th IEEE Photovoltaic Specialists Conference, IEEE, 2012, 001437–001441.

[30] L. Bouselham, B. Hajji, A. Mellit, A. Rabhi, A. Mazari, A reconfigurable pv

architecture based on new irradiance equalization algorithm, in: International Conference on Electronic Engineering and Renewable Energy, Springer, 2018, pp. 470–477.
[31] M. Balato, L. Costanzo, M. Vitelli, Reconfiguration of pv modules: a tool to get the best compromise between maximization of the extracted power and minimization of localized heating phenomena, Sol. Energy 138 (2016) 105–118.
[32] G. Spagnuolo, G. Petrone, B. Lehman, C.A.R. Paja, Y. Zhao, M.L.O. Gutierrez, Control of photovoltaic arrays: dynamical reconfiguration for fighting mismatched conditions and meeting load requests, IEEE industrial electronics magazine 9 (1) (2015) 62–76.
[33] D. La Manna, V.L. Vigni, E.R. Sanseverino, V. Di Dio, P. Romano, Reconfigurable electrical interconnection strategies for photovoltaic arrays: a review, Renew. Sustain. Energy Rev. 33 (2014) 412–426.
[34] D. Nguyen, B. Lehman, An adaptive solar photovoltaic array using model-based reconfiguration algorithm, IEEE Trans. Ind. Electron. 55 (7) (2008) 2644–2654.
[35] M. Baka, P. Manganiello, D. Soudris, F. Catthoor, A cost-benefit analysis for reconfigurable pv modules under shading, Sol. Energy 178 (2019) 69–78.
[36] X. Liu, Y. Wang, Reconfiguration method to extract more power from partially shaded photovoltaic arrays with series-parallel topology, Energies 12 (8) (2019) 1439.
[37] M. Alahmad, M.A. Chaaban, S. kit Lau, J. Shi, J. Neal, An adaptive utility interactive photovoltaic system based on a flexible switch matrix to optimize performance in real-time, Sol. Energy 86 (3) (2012) 951–963.
[38] G.J. Ward, The radiance lighting simulation and rendering system, in: Proceedings of the 21st Annual Conference on Computer Graphics and Interactive Techniques, 1994, pp. 459–472.
[39] R. Perez, P. Ineichen, R. Seals, J. Michalsky, R. Stewart, Modeling daylight availability and irradiance components from direct and global irradiance, Sol. Energy 44 (5) (1990) 271–289.
[40] D. Faiman, Assessing the outdoor operating temperature of photovoltaic modules, Prog. Photovoltaics Res. Appl. 16 (4) (2008) 307–315.
[41] D.L. King, J.A. Kratochvil, W.E. Boyson, Photovoltaic Array Performance Model, Tech. Rep, Sandia National Laboratories SAND2004-3535, 2004, https://doi.org/10.2172/919131.
[42] M. Wolf, G. Noel, R.J. Stirn, Investigation of the double exponential in the current—voltage characteristics of silicon solar cells, IEEE Trans. Electron. Dev. 24 (4) (1977) 419–428.
[43] J.-P. Charles, G. Bordure, A. Khoury, P. Mialhe, Consistency of the double exponential model with physical mechanisms of conduction for a solar cell under illumination, J. Phys. Appl. Phys. 18 (11) (1985) 2261.
[44] D.S. Chan, J.C. Phang, Analytical methods for the extraction of solar-cell single- and double-diode model parameters from iv characteristics, IEEE Trans. Electron. Dev. 34 (2) (1987) 286–293.
[45] K. Ishaque, Z. Salam, H. Taheri, et al., Modeling and simulation of photovoltaic (pv) system during partial shading based on a two-diode model, Simulat. Model. Pract. Theor. 19 (7) (2011) 1613–1626.
[46] A. Hovinen, Fitting of the solar cell iv-curve to the two diode model, Phys. Scripta (T54) (1994) 175, 1994.
[47] S. Guo, J. Singh, I. Peters, A. Aberle, T. Walsh, A quantitative analysis of photovoltaic modules using halved cells, Int. J. Photoenergy 2013 (2013).
[48] Ulbrich Solar Technologies, Multi tabbing wire. https://www.pvribbon.com/wp-content/uploads/Datasheets/MTW_Datasheet.pdf, 2018.
[49] ON Semiconductor, NVMFS6H800N MOSFET - power, single N-channel, rev 1, 2019. www.onsemi.com/pub/Collateral/NVMFS6H800N-D.PDF.
[50] ON Semiconductor, 80SQ045N Axial Lead Rectifier, Rev. 3, 2006. https://www.onsemi.com/pub/Collateral/80SQ045N-D.PDF.
[51] J. Remund, S. Müller, M. Schmutz, D. Barsotti, C. Studer, R. Cattin, Handbook Part I: Software, Meteotest, March 2020.
[52] H. Ziar, P. Manganiello, O. Isabella, M. Zeman, Photovoltatronics: intelligent pv-based devices for energy and information applications, Energy Environ. Sci. 14 (2021) 106–126.